Structure-Based Drug Discovery of IRE1 Modulators

Diana Pelizzari Raymundo, Leif A Eriksson, Eric Chevet, Xavier Guillory

Structure-based drug discovery of IRE1 modulators

Diana Pelizzari-Raymundo[1,2*], Leif A. Eriksson[3], Eric Chevet[1,2], Xavier Guillory[1,2,4*]

[1]INSERM U1242, Université de Rennes, Rennes, France. [2]Centre de Lutte contre le Cancer Eugène Marquis, Rennes, France. [3]Department of Chemistry and Molecular Biology, University of Gothenburg, Göteborg, Sweden. [4]Institut des Science Chimiques de Rennes, CNRS UMR6226, Université de Rennes, Rennes, France.

*corresponding authors – D. Pelizzari-Raymundo diana.pelizzari-raymundo@inserm.fr and X. Guillory xavier.guillory@univ-rennes1.fr

Keywords: Endoplasmic Reticulum • IRE1 • Unfolded Protein Response Computer assisted drug design (CADD) • Structure-based drug discovery (SBDD)

ABSTRACT

IRE1α (inositol requiring enzyme 1 alpha, referred to IRE1 hereafter) is an Endoplasmic Reticulum (ER) resident transmembrane enzyme with cytosolic kinase/RNAse activities. Upon ER stress IRE1 is activated through trans-autophosphorylation and oligomerization, resulting in a conformational change of the RNase domain thereby promoting two signaling pathways i) the non-conventional splicing of XBP1 mRNA and the regulated IRE1-dependent decay of RNA (RIDD). IRE1 RNase activity has been linked to diverse pathologies such as cancer or inflammatory, metabolic, and degenerative diseases and the modulation of IRE1 activity is emerging as an appealing therapeutic strategy against these diseases. Several modulators of IRE1 activity have been reported in the past, but none have successfully translated into the clinics as yet. Based on our expertise in the field, we describe in this chapter the approaches and protocols we used to discover novel IRE1 modulators and characterize their effect on IRE1 activity.

1. Introduction

1.1 The IRE1 pathway and its implication in diseases

There are three main ER stress sensors that transduce the Unfolded Protein Response from the ER lumen to the nucleus: The PKR-like ER kinase (PERK), the activating transcription factor 6 (ATF6) and the most evolutionarily conserved, the Inositol requiring enzyme 1 alpha (IRE1α, referred to as IRE1 hereafter) ***(1)***. Upon ER stress, IRE1 trans-autophosphorylates through its kinase domain and oligomerizes. This results in a conformational change that activates IRE1 RNase domain. These processes trigger two main signaling events namely the non-conventional splicing of X-box binding protein-1 (XBP1) splicing and regulated IRE1-dependent decay (RIDD) of RNA. The former initiates the unconventional splicing (together with the tRNA ligase RTCB) of XBP1 mRNA which in turn is translated into the XBP1 spliced (XBP1s) protein, a potent transcription factor whose target genes encode proteins involved in restoring ER homeostasis ***(2)***. RIDD instead triggers RNA degradation through RNA cleavage and action of cellular exonucleases ***(3)***. RIDD was shown to contribute to the degradation of ER-bound RNA in yeast and as such attenuate the entrance of newly synthesized proteins in the ER, thereby protecting this compartment ***(4)***. Alternatively, RIDD has also been involved in enhancing cell death mechanisms in case of terminal UPR through the degradation of mRNA encoding prosurvival factors ***(3)***.

In such context, the role of IRE1 in disease has been illustrated in many instances. IRE1 RNase activity has been shown to play important roles in tumorigenesis and tumor aggressiveness in many cancers (e.g. triple negative breast cancer, glioblastoma, myeloma, kidney, prostate, ovary, lung cancers amongst others) ***(5–8)***. XBP1s was found to be constitutively expressed in

several types of cancer and directly impact on tumorigenesis ***(9)***. Studies have shown that IRE1 inhibition in breast cancer ***(6, 8)***, prostate cancer ***(5)***, and glioblastoma ***(10)*** shows synergistic antitumor effects when combined with the current standards of care. In addition, hyper-activation of the IRE1-XBP1 axis in adipose tissue of obese humans has been related to adipose tissue macrophages polarization leading from an inactive metabolic state to an inflammatory activated phenotype (M1/M2) ***(11)***. ER stress and IRE1 signaling are also activated in nonalcoholic fatty liver disease (NAFLD), favoring the transition between steatosis and steatohepatitis (NASH). Studies have shown IRE1 RNase inhibitors prevented NASH via improvement of glucose tolerance ***(12)***. In the context of degenerative diseases, knockdown of XBP1 provides significant neuroprotection ***(13, 14)*** while deletion of IRE1 decreased the expression of amyloid precursor protein (APP) as well as amyloid β oligomers in cortical and hippocampal areas in mice model of AD ***(15)***. Similarly, reduced IRE1 RNase activity in the nervous system diminishes amyloid deposition and astrocyte activation, demonstrating that IRE1 has an important role in exacerbating neurodegenerative diseases ***(16)***. IRE1-XBP1s signaling has also been involved in the release of pro-inflammatory cytokines in myeloid cells ***(17)***. The binding of XBP1 on the promoters of both COX2 and PGES1 genes leads to their increased expression, thus promoting production and release of prostaglandins in leukocytes thus causing inflammatory pain ***(18)***. At last, some studies have observed a positive response against progression of atherosclerosis upon administration of IRE1 inhibitors in hyperlipidemic mice ***(19)***.

1.2 IRE1 activity modulation

In view of its broad-spectrum roles in diseases, interest in the modulation of IRE1 signaling has naturally developed and today represents an appealing therapeutic strategy. In this context, industrials and academics alike have worked on identifying and developing synthetic modulators of this trans-membrane dual kinase/RNase enzyme. Several potent and selective drug candidates were designed, but none has to date been successfully translated into the clinic.

[Figure 1 near here]

The IRE1 activity modulators reported in the literature can be classified as either activators or inhibitors and have been found to exert their effect by directly targeting either the RNase or Kinase domains (**Figure 1)**. Of note, the characterization of an allosteric relationship between the kinase and RNase domains has allowed for the modulation of IRE1 RNase activity with small molecules targeting the ATP-binding site, named kinase-inhibiting RNase attenuators (KIRAs) ***(20, 21)***. Most of these modulators, or their chemical starting points, have been identified in small to large screening campaigns. Exhaustive reviews on the discovery, efficacy and use of these different types of modulators can be found elsewhere ***(22–24)***. Our recent work on the structural exploration of the IRE1 kinase domain using active peptide fragments derived from the IRE1 cytosolic domain itself and molecular modeling tools led to the identification of several unreported IRE1 small-molecule inhibitors ***(25)***, thus demonstrating the relevance and applicability of a rational, structure-based approach.

The discovery of these novel modulators has been allowed by our in-house drug discovery pipeline (**Figure 2**; see in more detail in the method section below).

[Figure 2 near here]

In this chapter, we will focus on describing the procedures and protocols used successfully in our search of novel IRE1 modulators, ranging from molecular modeling, *in silico* screens, to biochemical and cell-based assays as well as *in vivo* validation.

2. Materials

2.1 Molecular Modeling

The primary prerequisites for docking experiments are: coordinate file(s) of the receptor protein; ligand libraries; and a molecular modeling program.

As of September 2020, there are a total of 13 human IRE1 and 8 yeast IRE1 crystal structures available freely (as pdb or mmCIF files) in the protein data bank (PDB) that can be used for molecular modeling. Careful consideration should be given to the choice of the structure and activation state of IRE1 that is captured in order to be relevant with the intended goal of the study (*see* **note 1 & 2**).

Numerous well-known libraries of small molecules are also available to the public for download, such as the ZINC15 database ***(26)***, ChEMBL ***(27)***, MolPort, and Enamine's REAL database. These libraries have become very large over the past few years and continuously cover more and more of the chemical space of synthetically tractable molecules. Therefore, a preliminary filtering for certain drug-like or molecular properties might be advised depending on the computational infrastructures available to perform virtual high-throughput screenings (VHTS). More specialized and smaller libraries of drug and drug-like molecules, sometimes annotated with bioactivities, can also be explored to obtain more advanced and lead-ready molecules. In this respect, the FDA repository of

approved drugs, the DrugBank databases, the NIH MLSMR and the Mcule libraries are often utilized.

Regarding the docking *per se*, a large number of docking programs can be used, but to only cite a handful of programs and software suites well-known for their performances, Schrodinger's Glide ***(28–30)***, AutoDock ***(31)*** and AutoDock Vina ***(32)***, VirtualFlow ***(33)***, GOLD ***(34)***, Molecular Operating Environment (MOE) ***(35)*** and BioSolveIT's FlexX ***(36)*** all represent robust options.

For our drug discovery projects targeting IRE1, we obtained excellent results for VHTS and advanced docking experiments with Schrodinger's Glide module (part of the Small-Molecule Drug Discovery suite, Schrödinger, LLC, New York, NY, 2018-4). In our recent work on peptidomimetic-based identification of compounds inhibiting IRE1 activity ***(25)***, the crystal structure of human IRE1 (*h*IRE1) in complex with its endogenous ligand ADP bound to the kinase site (PDB ID **3P23**)***(37)*** and the crystal structure of *h*IRE in complex with sulfonamide compound 18 (PDB ID **4U6R**) ***(38)*** were used as the starting point for all molecular modelling.

To summarize, for the molecular modeling and drug development phase the following resources were used:

1. Protein structure PDB ID 3P23 & 4U6R of *h*IRE1.

2. Library of overlapping tetra- and penta-peptides, based on the biologically active peptide 'P4', derived from IRE1 kinase domain ***(25, 39)***.

3. Library of FDA approved drugs.

4. Schrödinger software suite, in particular Protein Preparation Wizard, LigPrep, Glide (docking) and Phase (pharmacophores) modules.

5. Supercomputing resources (in this case supercomputer *Hebbe* at supercomputing center C3SE in Gothenburg; allocation of computing time generously provided through the Swedish National Infrastructure for Computing, SNIC).

2.2 RNase-mediated cleavage assay

1. Plate reader Tecan® infinite 200Pro.
2. 96 well plates flat bottom, black polystyrene, matrix active group High Bind (Corning®).
3. RNAse-free 1.5 mL tubes.
4. Buffer: 20 mM Hepes Buffer, pH 7.5; 1 mM MgOAc; 50 mM KOAc.
5. IRE1 recombinant protein (aa 465-977, His et GST Tag) Liquid (Sino Biological®).
6. Master mix solution (for each well – final volume 25 µL): 20 mM of ATP (Adenosine 5'-Triphosphate, Disodium Salt), 2 mM DTT solution (DL-Dithiothreitol ≥ 98 %), 1 µg of Fluorescent probe Cy3-CAUGUCCGCAGCGCAUG -BHQ3 (Eurogentec®) (See **note 10**), 14 µL of 20 mM Hepes Buffer, pH 7.5, 1 mM MgOAc, 50 mM KOAc.
7. Dimethyl sulfoxide (DMSO) anhydrous, ≥ 99.9 %.

2.3 Chemosensitization assay

1. Plate reader Tecan® infinite 200Pro.
2. Corning® 96 Well TC-Treated Microplates size 96 wells, polystyrene, flat bottom, sterile, lid.
3. DMEM, high glucose supplemented with Fetal Bovine Serum.
4. Trypsin-EDTA (0.05 %), phenol red.
5. PBS, pH 7.4.
6. Dimethyl sulfoxide (DMSO) anhydrous, ≥ 99.9 %.
7. 50 %, 6.1 N Trichloroacetic acid solution diluted in water.
8. 1 % Acetic acid diluted in water.
9. 0.04 % w/v of Sulforhodamine B sodium salt powder for cell culture diluted in 1 % acetic acid.
10. Tris buffer: 10 mM TrizmaBase, adjusted to pH10 with 5 N NaOH.

2.4 Quantification of XBP1 mRNA splicing in cells

1. Centrifuge 5427R.
2. Thermomixer® R, dry block heating and cooling shaker.
3. Corning® 6 Well TC-Treated Microplates size 6 wells, polystyrene, flat bottom, sterile, lid.
4. BRAND® 384-well PCR plate full skirt, cut corner A12, H12, white (Merck®).
5. QuantStudio™ 5 Real-Time PCR System, 384-well (Thermofisher™).

6. DMEM, high glucose supplemented with Fetal Bovine Serum.
7. Trypsin-EDTA (0.05 %), phenol red.
8. PBS, pH 7.4.
9. 5 mg/mL tunicamycin solution.
10. Trizol.
11. Chloroform.
12. Isopropanol.
13. Ethanol.
14. Ultra-pure DNase/RNase-Free Distilled Water.
15. TB Green® Premix Ex Taq™ (Tli RNase H Plus) (Takara Bio®).

3. Methods

3.1 Virtual drug discovery pipeline

Below is described a detailed presentation of the major steps of our virtual drug discovery pipeline using Schrodinger's Small Molecule Drug Discovery Suite. The interested reader can find additional extensive knowledge, training materials, and graphical or video tutorials accessible freely on Schrodinger's website ***(40)***.

3.2 IRE1 derived peptides preparation and docking

3.2.1 *In silico* protein preparation

Schrödinger's protein preparation wizard was used to prepare the crystal structure **3P23** and **4U6R** in a docking ready state ***(41)***, a process that includes multiple steps detailed hereafter.

1. Start the Protein Preparation Wizard by clicking on Task → Browse → Protein Preparation and Refinement → Protein Preparation Wizard, or alternatively by using the search taskbar.

2. *Import and process tab:*

   a. Import the structure into the workspace using its PDB ID (**3P23 & 4U6R**).

   b. In the pre-process box, in addition to the default settings, tick the following options:

      - Fill in missing side chains using Prime *(42)*.
      - Fill in missing loops using Prime *(43)*.
      - Delete waters beyond 5 Å from het groups

   c. Click 'Preprocess'.

3. *Review and modify tab:* Review the prepared structure for anomalies (*e.g.* water molecules, heteroatom groups states, etc.).

4. *Refine tab:*

a. Run the H-bond assignment with default settings.

b. Remove waters with fewer than 3 H-bonds to non-waters.

c. Run the restrained minimization with default settings.

d. After minimization, verify the protein report and Ramachandran plot.

e. If no major issues are raised, the model is ready for docking with Glide.

3.2.2 *In silico* ligands preparation

Similar to the protein preparation, the ligand preparation consists of a cascade of steps aiming at transforming the unprepared 1D, 2D or 3D structures of the input files into low-energy 3D structures ready for use in virtual screening.

1. Start the 'Ligand Preparation tool' by clicking on Task → Browse → Ligand Preparation and Library Design → LigPrep, or alternatively by using the search taskbar.

2. Import the unprepared ligand library (*see* **note 3**) containing the overlapping peptidic sequences (e.g. 1234; 2345; 3456; etc.) derived from the biologically active peptide 'P4' identified previously (18AAs, residues 701-718) ***(39)***.

3. Leave all settings on default and click 'Run'.

4. After preparation, a *filename*-out.maegz file containing all prepared structures ready for docking is obtained (*see* **note 4**).

3.2.3 Receptor grid generation

Similar to many other docking programs, Glide employs a grid-based approach to define a region of the receptor, for example a known binding site, in which the docking calculations are performed (**Figure 3**), thus shortening considerably the computation time.

[Figure 3 near here]

To identify the sequence within the P4 peptide responsible for the inhibitory activity, a structural exploration of IRE1 kinase pocket was carried out an unbiased docking of the short overlapping oligopeptides on the kinase domain. To this end, grids centered on the Kinase N-lobe domain were generated for each structure. These grids were set up as follow by using the Receptor Grid Generation module within Schrödinger.

1. Start the 'Receptor Grid Generation' tool by clicking on Task → Browse → Glide → Receptor Grid Generation, or alternatively use the search taskbar.

2. *Receptor tab:*

   a. The structures used here (i.e. **3P23 & 4U6R)** are receptor in complex with a ligand, therefore the ligand must be excluded from the grid generation (*see* **note 5**) by clicking on it in the workspace.

   b. For docking of peptide, such as the overlapping tetra- and pentapeptides used here (*see* **Figure 2**), the 'Generate grid suitable for peptide docking' option must be ticked (*see* **note 6**).

3. *Site tab:*

a. If a ligand was picked in the previous step, such as the ADP molecule from structure **3P23**, by default the grids are automatically centered on the centroid of the compound. So as to avoid bias, the centroid was chosen to be the center of the kinase N-lobe domain, rather than the ligand center, using the 'Centroid on selected residues' option.

b. For peptide docking, to take into account the ligand sizes, the sizes of the grids are adjusted using advanced options and the 'Dock ligands with length ≤' slider set to 30 Å (*see* **note 7**).

4. *Constraints tab:* This tab, which allow to set-up positional, NOE, H-bond, metal-ligand, and metal coordination constraints, was not used (*see* **note 8**).

5*. Rotatable Groups tab:* This option allows specific hydroxyl and thiol groups of Ser, Thr, Tyr and Cys residues to adopt different orientations depending on the ligand docked (*see* **note 9**). For instance, in the case of the grid centered on IRE1 kinase N-lobe, Thr584, Cys645, Thr648, Ser710 and Thr734 are non-buried residues located in or near the kinase pocket for which rotation can be allowed (**Figure 4**).

[Figure 4 near here]

6. Excluded Volumes tabs: As its name indicates, this tab allows the user to define regions of space where no atoms from the ligands are allowed to be docked. For our work on the discovery of novel IRE1 kinase inhibitors ***(25)***, this setting was not used as IRE1 kinase pocket is known for its flexibility and ability to accommodate ligands in the entire pocket.

7. *Grid generation:* Once the above parameters are properly configured, click ‘Run’ to generate the grid. A compressed .zip archive is generated in the job folder, ready for use in the Glide ligand docking step.

3.2.4 Peptide fragments docking

Following these preparatory steps, the peptides were docked into the grids prepared for each *h*IRE1 structure (PDB IDs 3P23 & 4U6R, respectively), along with their respective ligands: ADP and sulfonamide compound 18 ***(38)***.

1. Start the ‘Ligand Docking’ tool by clicking on Task → Browse → Glide → Ligand Docking, or alternatively by using the search taskbar.

2. Load the previously generated receptor grid suitable for peptide docking. Once loaded, Glide automatically select the ‘SP-peptide’ precision level in the ‘settings’ tab.

3. *Ligands tab:* Import the prepared ‘*filename*-out.maegz’ file generated by LigPrep.

4. All other settings and options were left on default.

5. Click ‘Run’ to start Glide.

6. After docking, a *filename*-pv.maegz file containing all docking poses is obtained and results are displayed in the workspace.

The best binding peptides were modified by replacing different sidechains (based on alanine scanning analysis) in order to optimize binding further. The novel set of modified peptides in all chiral and tautomeric forms were re-docked together with the parent peptide library and ADP with the same procedure. From this, the

two peptides F6P1 and F6P2 were identified as having better docking score than ADP, and selected for further work.

3.3 Pharmacophore hypotheses and filtering

The two candidate peptides in their binding poses in the 3P23 protein structure were used to generate pharmacophore models with the Phase program in Schrödinger. Filtering of the library of FDA approved compounds library was then performed against these pharmacophores, resulting in a reduced dataset suitable for further exploration.

1. Start the ‘Generate Pharmacophore Hypothesis’ tool by clicking on Task → Browse → Phase → Generate Pharmacophore Hypothesis, or alternatively by using the search taskbar.

2. Choose in the workspace the feature to include in the pharmacophore model (e.g. acceptors, donors, rings, etc.).

3. Click ‘Create’ to generate the pharmacophore hypothesis.

4. Start the ‘Ligand and Database Screening’ tool by clicking on Task → Browse → Phase → Ligand and Database Screening, or alternatively by using the search taskbar.

5. Load the prepared library of FDA approved drugs, generated as seen previously in section 3.1.1.2.

6. Select one or multiple pharmacophore models to screen against.

7. Click ‘Run’ to start Phase.

8. After filtering, a *filename*-hits.maegz file containing all molecules satisfying the criteria set is obtained and results are displayed in the workspace.

3.4 Virtual high-throughput screening

The reduced dataset of pharmacophore-filtered compounds was subjected to a final round of docking, this time at SP and XP level, towards the kinase pockets of PDB ID 3P23 and 4U6R, to identify compounds binding better than ATP, ADP or sulfonamide 18.

[Figure 5 near here]

Of the compounds obtained, only one FDA approved molecule (cephalosporine) resulted from the screening against the sulfonamide bound structure 4U6R, whereas all other were identified from the ADP-bound structure 3P23. Besides cephalosporine, three other compounds were identified from the database of FDA approved compounds: fludarabine phosphate, methotrexate (**Figure 5**) and folinic acid.

3.5 RNase-mediated cleavage *in vitro* assay

As previously described, IRE1 RNase cleaves unspliced XBP1 (XBP1u) mRNA at two conserved stem-loop sites and each site is located 3′ to a mirrored guanosine residue in the 7-base loop ***(44)***, to remove a 26-nucleotide intron. The two resulting exons are ligated by the tRNA ligase RtcB to produce spliced XBP1 (XBP1s) mRNA. Using a fluorescently tagged RNA oligonucleotide with the sequence corresponding to XBP1 mRNA endoribonuclease cleavage sites,

assays were performed as described below. The illustrative scheme of the assay is shown in **Figure 6**.

[Figure 6 near here]

1. Design the assay plates (**Figure 7)** with seven increasing concentrations of drugs to be tested as well as the positive and negative controls and the solution that was used to solubilize the drugs.

[Figure 7 here please]

2. Set up the method in the Tecan i-control application. The parameters are specified below:
    a. Excitation wavelength: 540 nm.
    b. Emission wavelength: 620 nm.
    c. Shaking before reading for 4 seconds in a linear mode.
    d. Readings: 25 times.
    e. Interval of readings: 1 min.
3. Pipette different volumes of drugs (and respective positive and negative controls) and buffer directly on the 96-well plate to a final volume of 22 µL per well.
4. Add 3 µg of IRE1 recombinant protein in each well.
5. Prepare a master mix.
6. Add 25 µL of master mix in each well.
7. Start the readings (See **note 11**).

The final data after normalization and calculation of the non-linear fit curve should have the appearance of the following curves showed on Figure 8 for IRE1 inhibitors (**Figure 8A**) and activators (**Figure 8B**), respectively.

[Figure 8 here please]

3.6 Chemosensitization assay

One of the main issues in cancer therapy lies in the fact that tumor cells might escape to the treatment, thereby becoming resistant. Since IRE1 signaling has been shown to exert pro-survival functions in tumor cells, we reasoned that the adjuvant alteration of IRE1 activation in cancer cells might enhance their sensitivity to current/standard treatments. In this context, we have the impact of compound-based IRE1 inhibition on the sensitivity of various cancer cell lines to known anticancer drugs.

3.6.1 Cell preparation and treatment

1. Design the plates (as showed in **Figure 9)** with increasing concentrations of drugs to be tested. Depending on the drugs and system tested, the drug concentration range should be adjusted based on literature and/or different set ups as preliminary data. As a negative control, one condition is treated similarly to the others, but with equal volumes of DMSO only.
2. Grow cells to desired level of confluency in a T75 flask in their standard Culture Medium (here used DMEM supplemented with FBS as described in materials).
3. Decant or aspirate the medium.

4. Add 2–3 mL fresh warm trypsin/EDTA solution. Transfer the flask to a 37 °C incubator.
5. Wash with warm PBS. Aspirate.
6. After 5 min, tap the side of the flask, and examine the flask under a microscope for lifting. If necessary, return the cells to the incubator for an additional 5–10 min, with occasional tapping, until lifting is complete.
7. Quickly quench the Trypsin reaction by adding 5–6 mL Complete Cell Culture Medium.
8. Transfer the cells to sterile 15 mL conical tubes.
9. Pellet the cells by centrifugation at 1500 x g for 3 min.
10. Decant the supernatant.
11. Wash the cells by pipetting 10 mL medium into each conical tube and resuspending the pellet. Collect the cells by centrifugation 1500 x g for 3 min.
12. Resuspend the washed cells in complete cell culture medium.
13. Enumerate cell density. For this application, the cell density should be adjusted to 50000 cells/mL cell culture medium.
14. Seed the cells (100 µL/well) in the culture medium in a 96-well plate in duplicate.
15. On the day 2, treat each condition with the drug (s) related to each condition.
16. Incubate at 37^{o}C; 5 % CO_2 for different time points (Usually 24, 48, 72 h).
17. Proceed with sulforhodamine B toxicity assay.

[Figure 9 here please]

3.6.2 Sulforhodamine B (SRB) assay

1. Add 50uL of 50 % TCA (diluted in water) per well.
2. Incubate 1 h at 4°C.
3. Wash 5 times with 200 µL of distilled water.
4. Dry the wells (by patting on tissues).
5. Add 50 µL of SRB solution (see **note 12**).
6. Incubate 30 min at room temperature in the dark.
7. Wash 5 times with 200 µL of acetic acid 1 %.
8. Dry the wells (by patting on tissues).
9. Add 100 µL of Tris-Base solution (stock solution: 10 mM – pH10).
10. Agitate 5 min.
11. Read the OD using 565 nm wavelength.
12. Calculate the percentage of living cells.

    The final data after normalization and calculation of the percentage of living cells should have the appearance of the following curves showed in Figure 10 depending of the effects of different treatments. Figure 10 shows one effective drug (named B) and a drug with no effect on the system tested (named A).

[Figure 10 here please]

3.7 Quantification of the expression of XBP1s and RIDD target mRNA

As previously described, IRE1 activation triggers two main pathways whose outputs will control life and death decision: the unconventional splicing of XBP1

mRNA and RIDD. To characterize the impact of the different IRE1 modulators on those outputs, we quantified the mRNA levels of XBP1s and RIDD targets under ER stress using quantitative RT-PCR (RT-qPCR).

3.7.1 Cells preparation and treatment

1. Grow cells to desired level of confluency in a T75 flask in their standard Culture Medium (here used DMEM supplemented with FBS as described in materials).
2. Decant or aspirate the medium.
3. Add 2–3 mL fresh warm trypsin/EDTA solution. Transfer the flask to a 37°C incubator.
4. Wash with warm PBS. Aspirate.
5. After 5 min, tap the side of the flask, and examine the flask under a microscope for lifting. If necessary, return the cells to the incubator for an additional 5–10 min, with occasional tapping, until lifting is complete.
6. Quickly quench the Trypsin reaction by adding 5–6 mL Complete Cell Culture Medium.
7. Transfer the cells to sterile 15 mL conical tubes.
8. Pellet the cells by centrifugation at 1500 x g for 3 min.
9. Decant the supernatant.
10. Wash the cells by pipetting 10 mL medium into each conical tube and resuspending the pellet. Collect the cells by centrifugation 1500 x g for 3 min.
11. Resuspend the washed cells in complete cell culture medium.

12. Enumerate cell density. For this application, the cell density should be adjusted to 50000 cells/mL cell culture medium.
13. Seed the cells in the usual medium (2 mL/well) in a 6-well plate.
14. Treat in each condition with your drugs, molecules or peptides and add the ER stressor (see note 13).
15. Incubate at 37ºC, 5 % CO_2 for different time points.

3.7.2 RNA extraction

1. Add 1 mL of Trizol reagent in each well.
2. Keep at -20ºC until start the RNA extraction protocol.
3. Transfer the Trizol solution to a 1.5 mL tube.
4. Add 200 µL of chloroform.
5. Mix by inversion.
6. Leave to rest at room temperature for 10 min.
7. Spin at 12000 rpm, 4ºC for 15 min (see note 14).
8. Take aqueous phase.
9. Add 500 µL of isopropanol (see note 15).
10. Mix by inversion 5 times.
11. Leave to rest at room temperature.
12. Spin at 120000 rpm, 4 °C for 10 min.
13. Discard supernatant.
14. Add 1 mL of Ethanol 75 %.
15. Repeat steps 12 and 13.

16. Discard supernatant.
17. Add 500 µL of Ethanol 75 %.
18. Repeat steps 12 and 13.
19. Remove all the liquid using a pipette.
20. Dry the pellet by evaporation.
21. Add 20 µL of distilled water.
22. Heat at 55 °C for 10 min.
23. Quantify the RNA.

3.7.3 RT-PCR and qPCR

The protocols must be carried out as described in the datasheet provided by the manufacturers. Here we used Reverse Transcriptase Maxima (Thermofisher^{TM}) and TB Green Premix Ex Taq II (Tli RNase H Plus) (Takara Bio®).

[Figure 11 near here]

In **Figure 11** we show the dose-dependent effect of the drug after the treatment with increased concentrations of the molecule (**Figure 11A**) or a time course with and without the drug both in the presence of Tunicamycin in order to identify the timeline of ER stress inhibition by the drug (**Figure 11B**).

Once these different levels completed, one can envision *in vivo* experiments in various models of cancer as previously described by us ***(10, 45)***.

4. Notes

1. IRE1 activation mechanism in response to the disruption of endoplasmic reticulum (ER) homeostasis (e.g. triggered by the accumulation of improperly

folded proteins) is complex. Briefly, IRE1 trans-autophsophorylates triggering a formation of a face to face dimer which undergoes a conformational change to a different dimer form (back to back) for which oligomerisation occurs. Upon formation of the back to back dimer, the RNase site takes its appropriate active form (i.e. is made up of two halves, one from each monomer, coming together). The comprehension of this chain of event was notably made possible by the obtention of crystal structures capturing IRE1 in its different states of activation ***(46, 47)***. Choosing the crystal structure of IRE1 that is in accordance with the purpose of the molecular modelling work is therefore critically important.

2. Depending on the activation state of IRE1 studied, the crystal structures available might contain multiple protein chains in the crystal asymmetric unit. Therefore, careful attention should be paid to the quality criteria of each chain, and especially of the binding site of interest, such as B-factor, occupancy, binding site waters, missing loops, residues and side chains, Ramachandran outliers, etc. Choosing the best structure available is critical for the success of the virtual screens since most docking protocols keep the receptor rigid during the docking experiments ***(48)***.

3. Compatible ligand library file formats for LigPrep are .sdf files, .mol files, SMILES codes (.smi or stored in a .csv table) or .mae files (Maestro proprietary files).

4. Depending on the input molecular structures and options selected, multiple output structures can be obtained at the end of this process (tautomers, stroisomers, etc.).

5. During the receptor grid generation, it is important to know that everything not defined as the "ligand" is treated as part of the receptor, including ions, cofactors and water molecules. This is for example the case with structure **3P23** where an ADP molecule and a Mg^{2+} ion, serving as cofactor coordinating the phosphate group, are bound in the kinase pocket. During the receptor grid generation, only the ADP molecule (but not the Mg^{2+} ion) is defined as ligand by the software and ignored from the grid. It is therefore important that ions, co-factors, non-bridging waters or crystallization salts present in the cubic volume of the grid are deleted prior to grid generation.

6. Grids suitable for peptide docking use slightly altered parameters and a different scoring function***(49)*** compared to grid generated for small-molecules docking with Glide simple precision (SP) and/or extra precision (XP) modes, and can only be used in SP-peptide mode.

7. Glide grids rely on two boxes (**Figure 3**) to define ligand mobility in the docking stage: the *enclosing box*, which is the larger box in which the ligands are confined, and the smaller *inner box* in which the ligand center is allowed to move (also called *ligand diameter midpoint box)*. The sizes of these two boxes are therefore critically important and should be carefully considered depending on the size of the ligands to dock. If a ligand was picked in the precedent step, Glide assumes by default that the ligands to dock are similar in size and accordingly adjusts the enclosing box. However, if the ligand libraries contain significantly larger or smaller molecules, the enclosing box size should be adjusted using the ‘Dock ligands with length ≤’ slider.

8. Constraints are interesting if specific receptor-ligand interactions are targeted or known to be important to the binding mode (*e.g.* lead optimization of a ligand co-crystallized with its receptor). Such constraints can also significantly improve the reliability of the output docking poses and speed up docking by discarding early-on in the process ligands and conformations that do not fulfill the specified criteria. In this case, due to the absence of experimental evidences on binding mode (SAR, crystal structure(s), etc.), this field was left blank.

9. Flexibility of hydroxyl and thiol groups in the receptor come at a slight cost in computational time but produce improved results by finding the most favorable ligand-receptor interactions. The choice of groups for which to allow rotation can be made by visually inspecting their relevance to the docking experiment. For instance, allowing rotation only to groups located in close proximity of the ligand or binding site studied is a sensible choice.

10. Resuspend the probe to a concentration of 1 µg/µL, which depends on the amount received from the company.

11. In order to minimize the delay between the start of the enzyme activity and the readings, add the master mix as quick as possible with a multi-channel or automatic pipette.

12. Keep the SFB stock solution protected from light.

13. ER stress induction can be achieved using different ER stressors such as Tunicamycin, Thapsigargin and DTT. The intensity of ER stress can also be modulated in function of the time of treatment and the concentration of the ER stressor. Here, for a mild stress we treated the cells with 1µg/mL of Tunicamycin for a timeline incubation (0, 2, 4, 8, 16 and 24 h).

14. After centrifugation 2 phases will clear appear. The aqueous phase where is the RNA and the phenolic phase. The step of taking the aqueous phase should be done carefully to do not contaminate your sample with phenol, which could compromise the quality of your final RNA sample.

15. Use 1.5 mL tube since it is difficult to see the pellet in larger tubes.

5. Acknowledgements

This work was funded by grants from Institut National de la Santé et de la Recherche Médicale (INSERM), Institut National du Cancer (INCa, PLBIO2017, 18, 19, 20), Fondation pour la Recherche Médicale (FRM, équipe labellisée 2018), Agence National de la Recherche (ANR, eRaNet ERAAT, IRE1inNASH) to EC. DPR was funded by INSERM (LA VANNETAISE). LAE acknowledge the support of The Swedish Research Council (Vetenskapsrådet), grant no 2019-3684, and the Swedish National Infrastructure for Computing (SNIC) for access to supercomputing resources of the supercomputing centre C3SE in Gothenburg. This work has also been supported by the Fondation ARC pour la recherche sur le cancer, grant PDF20191209830, to XG.

6. References

1. Xue Z, He Y, Ye K, et al (2011) A Conserved Structural Determinant Located at the Interdomain Region of Mammalian Inositol-requiring Enzyme 1α. J Biol Chem 286:30859–30866

2. Hetz C, Chevet E, Oakes SA (2015) Proteostasis control by the unfolded protein response. Nat Cell Biol 17:829–838

3. Maurel M, Chevet E, Tavernier J, Gerlo S (2014) Getting RIDD of RNA: IRE1 in cell fate regulation. Trends in Biochemical Sciences 39:245–254

4. Guydosh NR, Kimmig P, Walter P, Green R (2017) Regulated Ire1-dependent mRNA decay requires no-go mRNA degradation to maintain endoplasmic reticulum homeostasis in S. pombe. eLife 6:e29216

5. Sheng X, Nenseth HZ, Qu S, et al (2019) IRE1α-XBP1s pathway promotes prostate cancer by activating c-MYC signaling. Nature Communications 10:323

6. Logue SE, McGrath EP, Cleary P, et al (2018) Inhibition of IRE1 RNase activity modulates the tumor cell secretome and enhances response to chemotherapy. Nature Communications 9:3267

7. Lhomond S, Avril T, Dejeans N, et al (2018) Dual IRE1 RNase functions dictate glioblastoma development. EMBO Molecular Medicine 10:e7929

8. Zhao N, Lewis MT, Chen X, et al (2018) Pharmacological targeting of MYC-regulated IRE1/XBP1 pathway suppresses MYC-driven breast cancer. The Journal of clinical investigation 128:1283–1299

9. Storm M, Sheng X, Arnoldussen YJ, Saatcioglu F (2016) Prostate cancer and the unfolded protein response. Oncotarget 7:54051–54066

10. Le Reste PJ, Pineau R, Voutetakis K, et al (2020) Local intracerebral inhibition of IRE1 by MKC8866 sensitizes glioblastoma to irradiation/chemotherapy in vivo. Cancer Letters 494:73–83

11. Shan B, Wang X, Wu Y, et al (2017) The metabolic ER stress sensor IRE1α suppresses alternative activation of macrophages and impairs energy expenditure in obesity. Nature Immunology 18:519–529

12. Lebeaupin C, Vallée D, Rousseau D, et al (2018) Bax inhibitor-1 protects from nonalcoholic steatohepatitis by limiting inositol-requiring enzyme 1 alpha signaling in mice. Hepatology 68:515–532

13. Medinas DB, González J V., Falcon P, Hetz C (2017) Fine-tuning ER stress signal transducers to treat amyotrophic lateral sclerosis. Frontiers in Molecular Neuroscience 10:216

14. Kiskinis E, Sandoe J, Williams LA, et al (2014) Pathways disrupted in human ALS motor neurons identified through genetic correction of mutant SOD1. Cell Stem Cell 14:781–795

15. Duran-Aniotz C, Cornejo VH, Espinoza S, et al (2017) IRE1 signaling exacerbates Alzheimer's disease pathogenesis. Acta Neuropathol 134:489–506

16. Duran-Aniotz C, Cornejo VH, Espinoza S, et al (2017) IRE1 signaling exacerbates Alzheimer's disease pathogenesis. Acta Neuropathologica 134:489–506

17. Martinon F, Chen X, Lee A-H, Glimcher LH (2010) TLR activation of the transcription factor XBP1 regulates innate immune responses in macrophages. Nature Immunology 11:411–418

18. Chopra S, Giovanelli P, Alvarado-Vazquez PA, et al (2019) IRE1α–XBP1 signaling in leukocytes controls prostaglandin biosynthesis and pain. Science 365:eaau6499

19. Tufanli O, Telkoparan Akillilar P, Acosta-Alvear D, et al (2017) Targeting IRE1 with small molecules counteracts progression of atherosclerosis. Proceedings of the National Academy of Sciences 114:E1395–E1404

20. Wang L, Perera BGK, Hari SB, et al (2012) Divergent allosteric control of the IRE1α endoribonuclease using kinase inhibitors. Nature Chemical Biology 8:982–989

21. Feldman HC, Tong M, Wang L, et al (2016) Structural and Functional Analysis of the Allosteric Inhibition of IRE1α with ATP-Competitive Ligands. ACS Chem Biol 11:2195–2205

22. Raymundo DP, Doultsinos D, Guillory X, et al (2020) Pharmacological Targeting of IRE1 in Cancer. Trends in Cancer. doi:10.1016/j.trecan.2020.07.006

23. Grandjean JMD, Wiseman RL (2020) Small molecule strategies to harness the unfolded protein response: where do we go from here? J Biol Chem jbc.REV120.010218

24. Hetz C, Axten JM, Patterson JB (2019) Pharmacological targeting of the unfolded protein response for disease intervention. Nature Chemical Biology 15:764–775

25. Doultsinos D, Carlesso A, Chintha C, et al Peptidomimetic-based identification of FDA approved compounds inhibiting IRE1 activity. The FEBS Journal. doi: 10.1111/febs.15372

26. Sterling T, Irwin JJ (2015) ZINC 15 – Ligand Discovery for Everyone. J Chem Inf Model 55:2324–2337

27. Gaulton A, Hersey A, Nowotka M, et al (2017) The ChEMBL database in 2017. Nucleic Acids Res 45:D945–D954

28. Friesner RA, Banks JL, Murphy RB, et al (2004) Glide: A New Approach for Rapid, Accurate Docking and Scoring. 1. Method and Assessment of Docking Accuracy. J Med Chem 47:1739–1749

29. Halgren TA, Murphy RB, Friesner RA, et al (2004) Glide: A New Approach for Rapid, Accurate Docking and Scoring. 2. Enrichment Factors in Database Screening. J Med Chem 47:1750–1759

30. Friesner RA, Murphy RB, Repasky MP, et al (2006) Extra Precision Glide: Docking and Scoring Incorporating a Model of Hydrophobic Enclosure for Protein−Ligand Complexes. J Med Chem 49:6177–6196

31. Morris GM, Huey R, Lindstrom W, et al (2009) AutoDock4 and AutoDockTools4: Automated Docking with Selective Receptor Flexibility. J Comput Chem 30:2785–2791

32. Trott O, Olson AJ (2010) AutoDock Vina: improving the speed and accuracy of docking with a new scoring function, efficient optimization and multithreading. J Comput Chem 31:455–461

33. Gorgulla C, Boeszoermenyi A, Wang Z-F, et al (2020) An open-source drug discovery platform enables ultra-large virtual screens. Nature 580:663–668

34. Jones G, Willett P, Glen RC, et al (1997) Development and validation of a genetic algorithm for flexible docking11Edited by F. E. Cohen. Journal of Molecular Biology 267:727–748

35. Molecular Operating Environment (MOE), 2019.01; Chemical Computing Group ULC, 1010 Sherbooke St. West, Suite #910, Montreal, QC, Canada, H3A 2R7, 2020. https://www.chemcomp.com/Products.htm. Accessed 14 Sep 2020

36. Rarey M, Kramer B, Lengauer T, Klebe G (1996) A fast flexible docking method using an incremental construction algorithm. J Mol Biol 261:470–489

37. Ali MMU, Bagratuni T, Davenport EL, et al (2011) Structure of the Ire1 autophosphorylation complex and implications for the unfolded protein response. The EMBO Journal 30:894–905

38. Harrington PE, Biswas K, Malwitz D, et al (2015) Unfolded Protein Response in Cancer: IRE1α Inhibition by Selective Kinase Ligands Does Not Impair Tumor Cell Viability. ACS Med Chem Lett 6:68–72

39. Bouchecareilh M, Higa A, Fribourg S, et al (2011) Peptides derived from the bifunctional kinase/RNase enzyme IRE1α modulate IRE1α activity and protect cells from endoplasmic reticulum stress. The FASEB Journal 25:3115–3129

40. Training | Schrödinger. https://www.schrodinger.com/training. Accessed 15 Sep 2020

41. Madhavi Sastry G, Adzhigirey M, Day T, et al (2013) Protein and ligand preparation: parameters, protocols, and influence on virtual screening enrichments. J Comput Aided Mol Des 27:221–234

42. Jacobson MP, Friesner RA, Xiang Z, Honig B (2002) On the Role of the Crystal Environment in Determining Protein Side-chain Conformations. Journal of Molecular Biology 320:597–608

43. Jacobson MP, Pincus DL, Rapp CS, et al (2004) A hierarchical approach to all-atom protein loop prediction. Proteins: Structure, Function, and Bioinformatics 55:351–367

44. Volkmann K, Lucas JL, Vuga D, et al (2011) Potent and Selective Inhibitors of the Inositol-requiring Enzyme 1 Endoribonuclease. J Biol Chem 286:12743–12755

45. Logue SE, McGrath EP, Cleary P, et al (2018) Inhibition of IRE1 RNase activity modulates the tumor cell secretome and enhances response to chemotherapy. Nat Commun 9:3267

46. Korennykh A, Walter P (2012) Structural Basis of the Unfolded Protein Response. Annual Review of Cell and Developmental Biology 28:251–277

47. Korennykh AV, Egea PF, Korostelev AA, et al (2009) The unfolded protein response signals through high-order assembly of Ire1. Nature 457:687–693

48. Biesiada J, Porollo A, Meller J (2012) On Setting Up and Assessing Docking Simulations for Virtual Screening. In: Zheng Y (ed) Rational Drug Design: Methods and Protocols. Humana Press, Totowa, NJ, pp 1–16

49. Tubert-Brohman I, Sherman W, Repasky M, Beuming T (2013) Improved Docking of Polypeptides with Glide. J Chem Inf Model 53:1689–1699

Figure 1. ***Mode of action of synthetic IRE1 modulators.*** *KIRA, RNAse (MKC) and ATP binding pocket inhibitors (AI) are shown in the figures as well as the region in which they bind IRE1. Other molecules such as APY29 (Kinase activator) and IXA4 (RNase activator) are known to bind and induce IRE1 activities. The dashed arrow represents a predicted drug-target interaction.*

Figure 2: ***In-house drug discovery pipeline for the discovery of IRE1 modulators.*** *Starting from peptidic fragments derived from IRE1 kinase domain known to have inhibitory activity* ***(39)****, libraries of oligopeptides were generated (step 1), docked and the best binders were optimized (step 2). Pharmacophore hypotheses were then defined and used to filter the FDA library of approved drugs, resulting in a reduced dataset of small molecules that were redocked and ranked (step 3). Top ranking candidates, along with the optimized oligopeptides, were tested in vitro for their capacity to alter IRE1 RNase activity, followed by cell and in vivo studies for the most promising hits. The rationale behind the development of this drug discovery pipeline is laid out in detail in the publication associated with the discovery of these novel inhibitors* ***(25)****.*

Figure 3. ***Grid boxes in molecular docking with Glide.*** *Illustration of the larger enclosing box (magenta) containing the inner box (green) and centered on the centroid of the ADP molecule (limegreen, stick and ball representation) bound into IRE1 kinase pocket. Note the presence of a* MG^{2+} *ion (pink, CPK representation) near the ligand that must be deleted before grid generation.*

Figure 4. ***Rotatable groups in grid generation.*** *Residues (grey, stick representation) within the hIRE1 kinase pocket (cartoon representation, grey surface) with relevant rotatable OH and SH groups.*

Figure 5. ***Methotrexate bound to IRE1 kinase pocket. A.*** *Best docking pose of methotrexate (green, ball and stick) bound to the kinase pocket of structure 3P23 of hIRE1 (grey, stick representation; cartoon backbone).* ***B.*** *Ligand interaction diagram of methotrexate bound to hIRE1 kinase pocket.*

Figure 6. ***Endoribonuclease assay scheme for IRE1-mediated mRNA XBP1 cleavage.*** *The fluorescent dye Cy5® is quenched by the black hole BHQ®-2 and linked by the mini-XBP-1 stem-loop. When IRE1 cleaves the mRNA XBP1 in its specific site the quencher is secluded from the dye and the fluorescence can be emitted.*

Figure 7. ***96-well template for drug screening by RNAse in vitro cleavage assay.***

Figure 8. ***RNase-mediated in vitro cleavage assay for IRE1 inhibitors (A) and activators (B), respectively.*** *The values of fluorescence in each condition were plotted and analyzed using GraphPad Prism 8. After linear regression analysis, IC_{50} or EC_{50} were calculated for each molecule.*

Figure 9. ***96-well plate template for chemosensitization assays.*** *Increasing concentrations of each drug are added through the columns. Buffer and different molecules (represented in the picture as A, B, C…) were combined with the main drug(s) used in the clinic.*

Figure 10. ***Chemosensitization assay results.*** *Representative results after a chemosensitization assay. As showed in the figure, no effect was seen between drug alone and buffer or molecule A. However, molecule B has a strong effect sensitizing the cells to the treatment with the drug.*

Figure 11. ***mRNA levels determination for XBP1s and RIDD targets.*** *Representative results of qPCR assay. Panel* ***A.*** *shows the increasing of degradation of RIDD mRNA levels after the treatment with tunicamycin (Tun). The inhibition of degradation is dose-dependent after the treatment with molecule.* ***B.*** *A time course treatment with Tunicamycin (black line) and Tunicamycin with molecule B (green line) was performed for 24 h. Molecule B inhibits the splicing of XBP1 mRNA induced by Tunicamycin*.

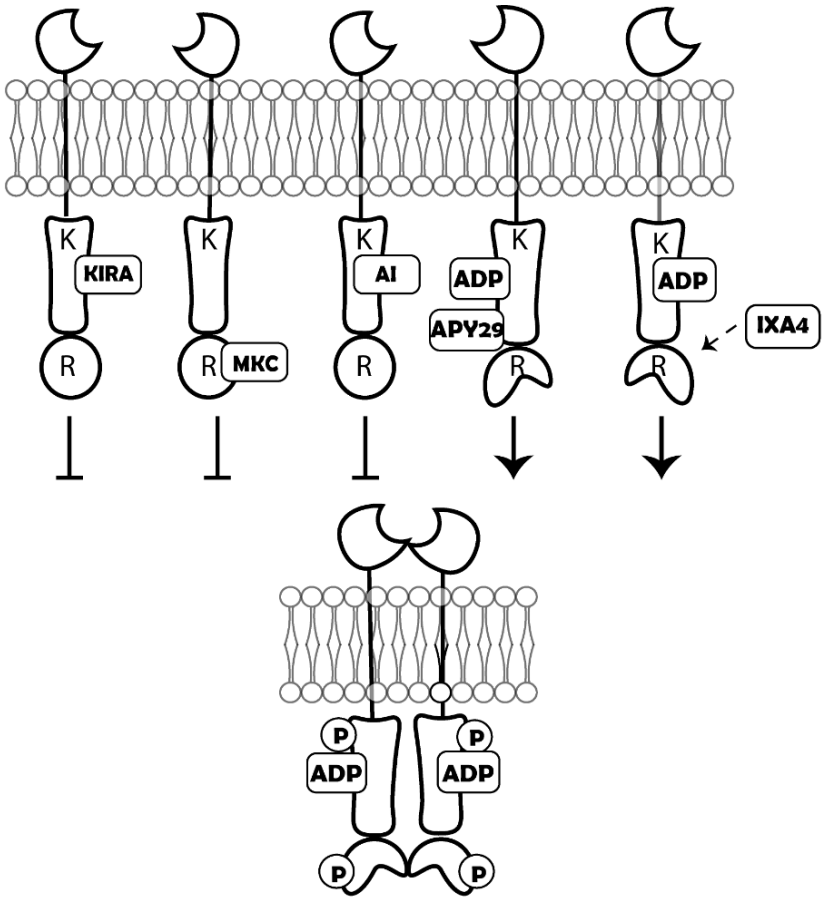

Figure 1. ***Mode of action of synthetic IRE1 modulators.*** *KIRA, RNAse (MKC) and ATP binding pocket inhibitors (AI) are shown in the figures as well as the region in which they bind IRE1. Other molecules such as APY29 (Kinase activator) and IXA4 (RNase activator) are known to bind and induce IRE1 activities. The dashed arrow represents a predicted drug-target interaction.*

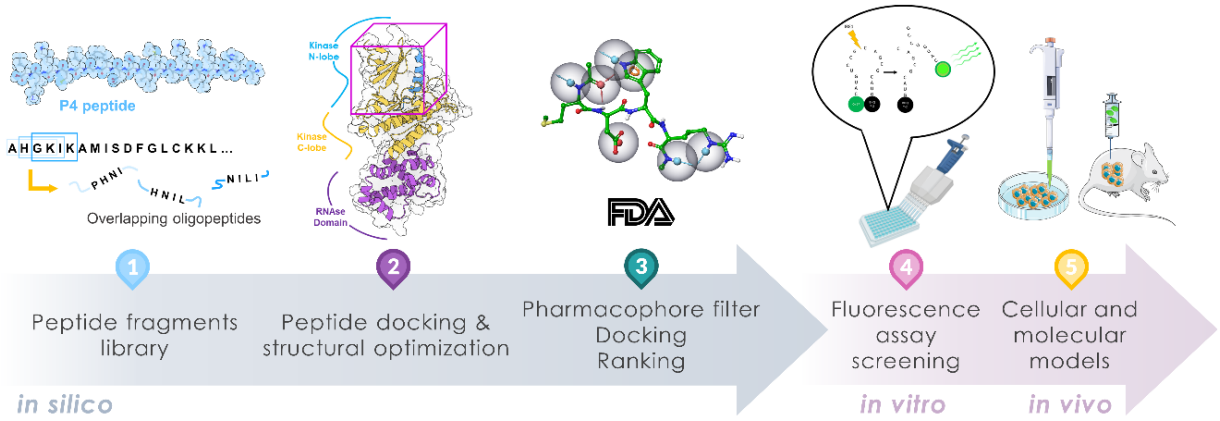

Figure 2: ***In-house drug discovery pipeline for the discovery of IRE1 modulators.*** *Starting from peptidic fragments derived from IRE1 kinase domain known to have inhibitory activity* ***(1)****, libraries of oligopeptides were generated (step 1), docked and the best binders were optimized (step 2). Pharmacophore hypotheses were then defined and used to filter the FDA library of approved drugs, resulting in a reduced dataset of small molecules that were redocked and ranked (step 3). Top ranking candidates, along with the optimized oligopeptides, were tested in vitro for their capacity to alter IRE1 RNase activity, followed by cell and in vivo studies for the most promising hits. The rationale behind the development of this drug discovery pipeline is laid out in detail in the publication associated with the discovery of these novel inhibitors* ***(2)****.*

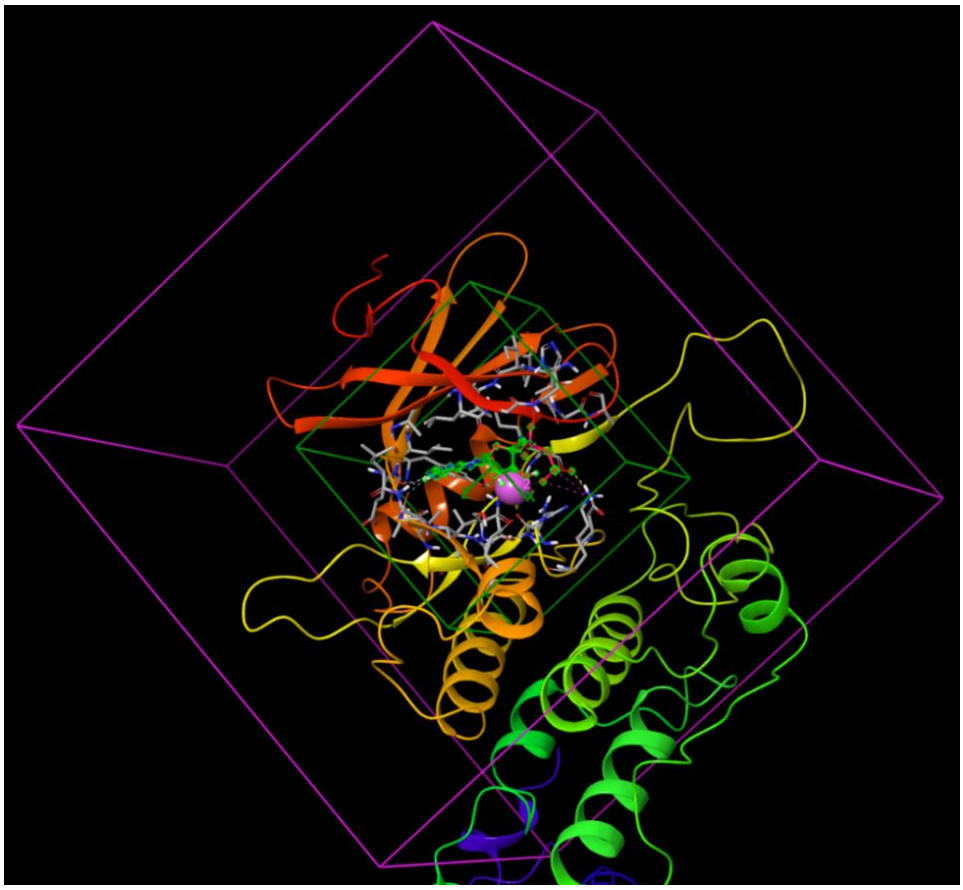

Figure 3. ***Grid boxes in molecular docking with Glide.*** *Illustration of the larger enclosing box (magenta) containing the inner box (green) and centered on the centroid of the ADP molecule (limegreen, stick and ball representation) bound into IRE1 kinase pocket. Note the presence of a* MG^{2+} *ion (pink, CPK representation) near the ligand that must be deleted before grid generation.*

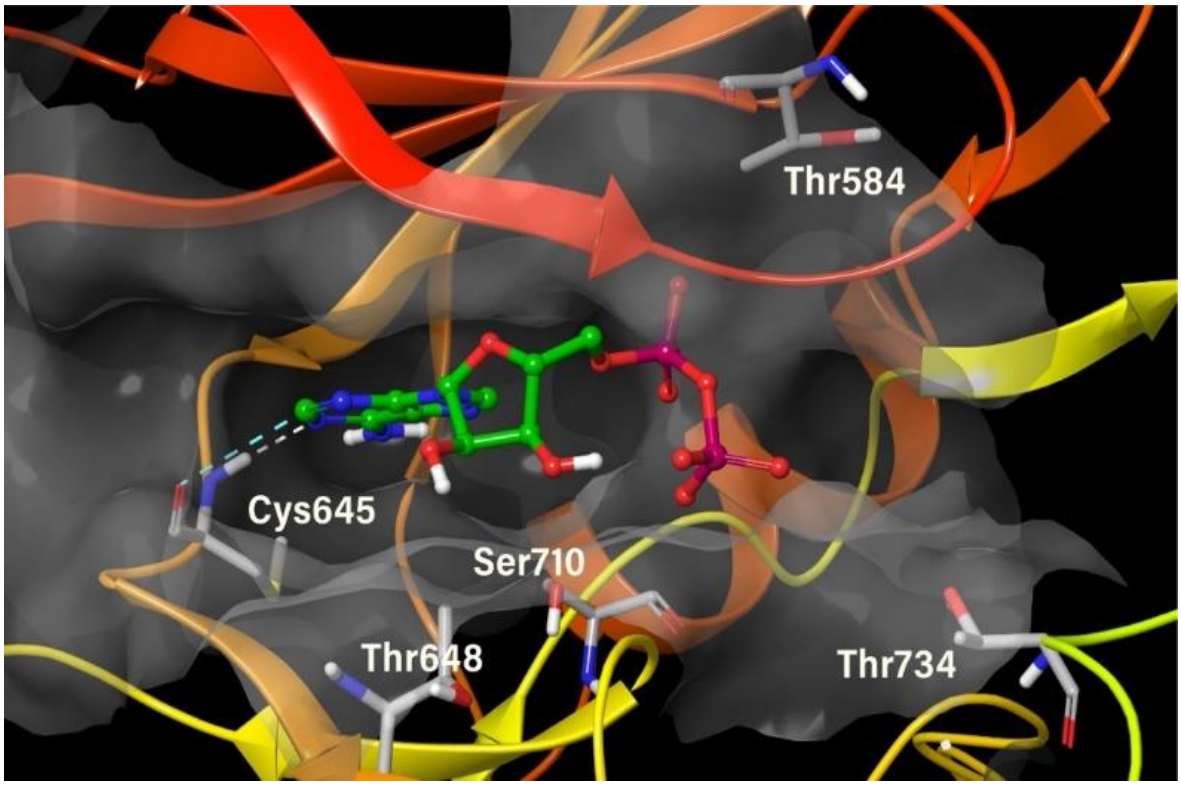

Figure 4. ***Rotatable groups in grid generation.*** *Residues (grey, stick representation) within the hIRE1 kinase pocket (cartoon representation, grey surface) with relevant rotatable OH and SH groups.*

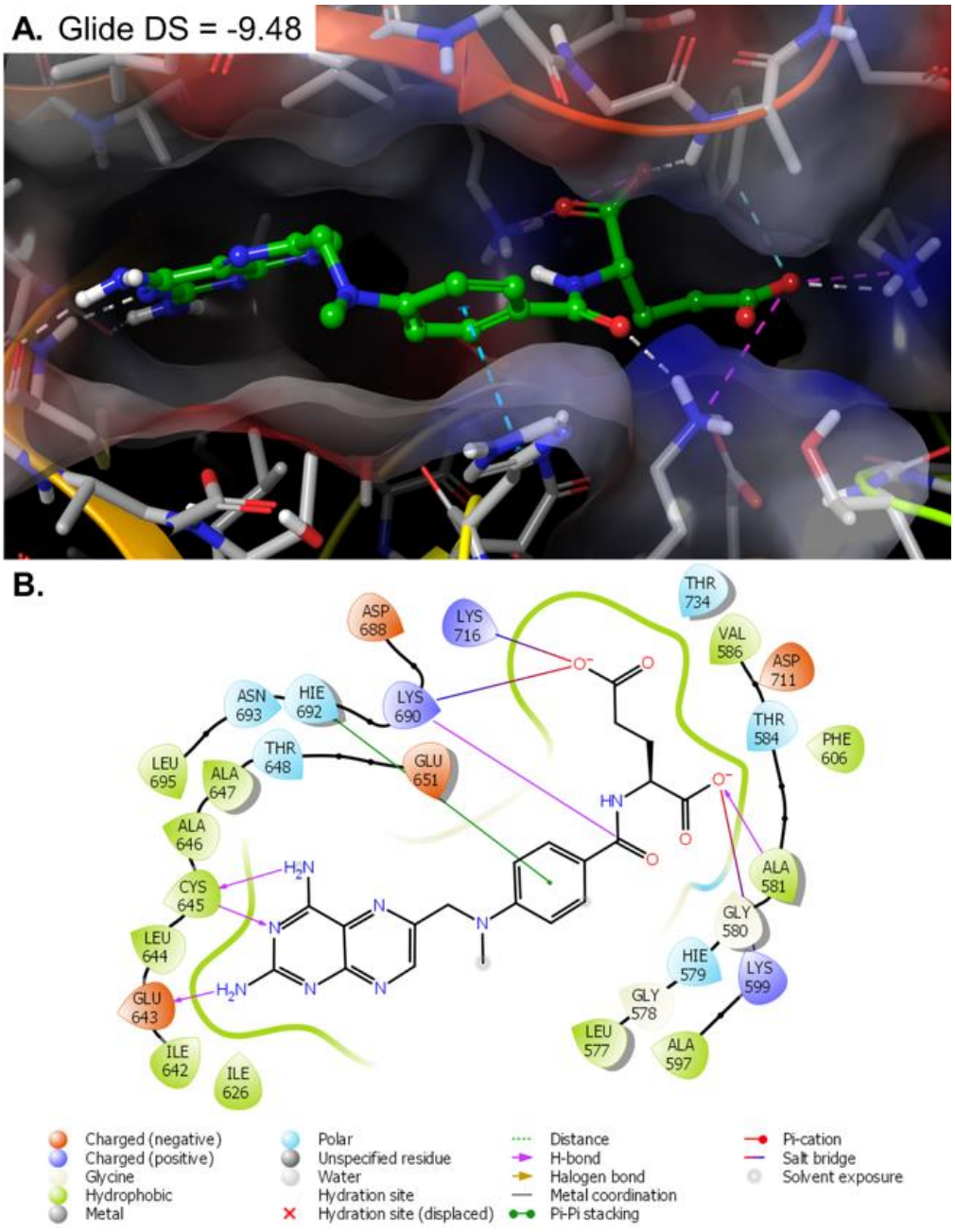

Figure 5. ***Methotrexate bound to IRE1 kinase pocket. A.*** *Best docking pose of methotrexate (green, ball and stick) bound to the kinase pocket of structure 3P23 of hIRE1 (grey, stick representation; cartoon backbone).* ***B.*** *Ligand interaction diagram of methotrexate bound to hIRE1 kinase pocket.*

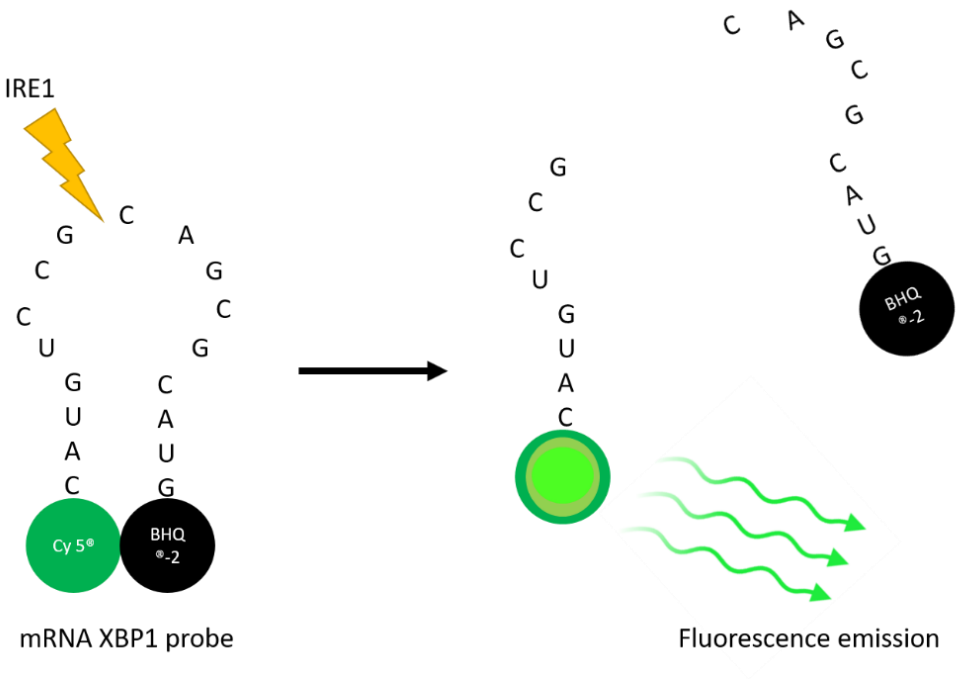

Figure 6. ***Endoribonuclease assay scheme for IRE1-mediated mRNA XBP1 cleavage.*** *The fluorescent dye Cy5® is quenched by the black hole BHQ®-2 and linked by the mini-XBP-1 stem-loop. When IRE1 cleaves the mRNA XBP1 in its specific site the quencher is secluded from the dye and the fluorescence can be emitted.*

7. 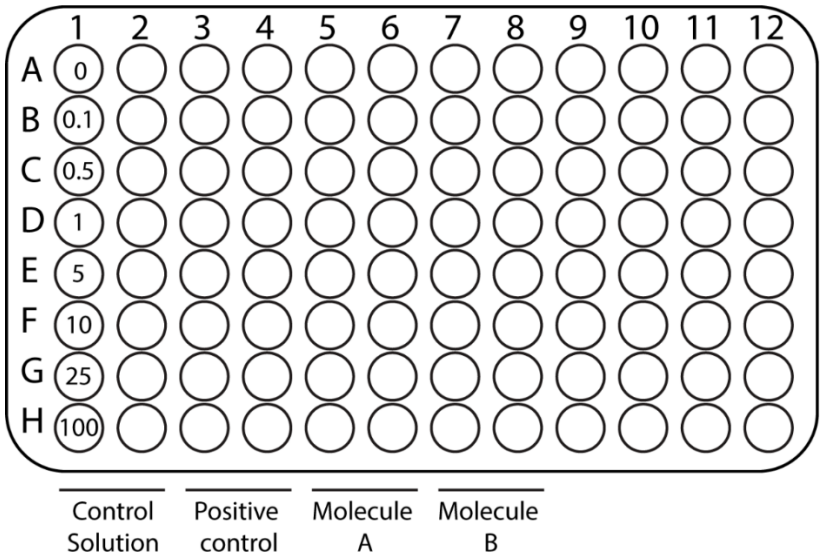

8. **Figure 7.** ***96-well template for drug screening by RNAse in vitro cleavage assay.***

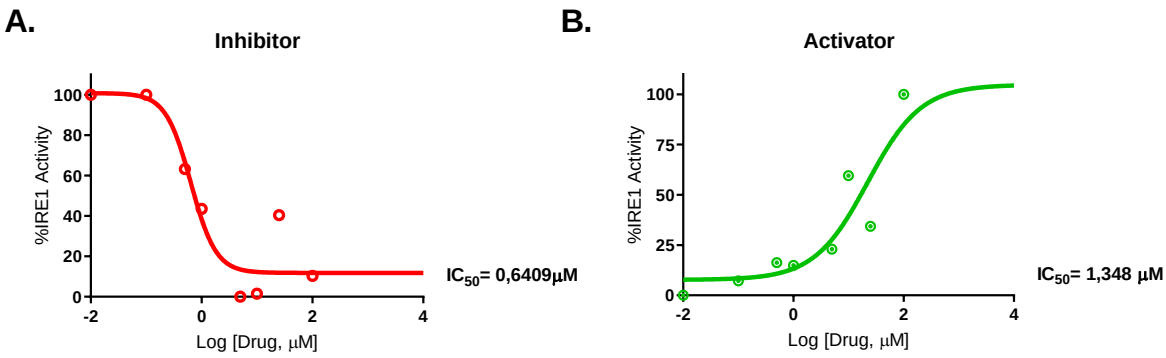

Figure 8. ***RNase-mediated in vitro cleavage assay for IRE1 inhibitors (A) and activators (B), respectively.*** *The values of fluorescence in each condition were plotted and analyzed using GraphPad Prism 8. After linear regression analysis, IC_{50} or EC_{50} were calculated for each molecule.*

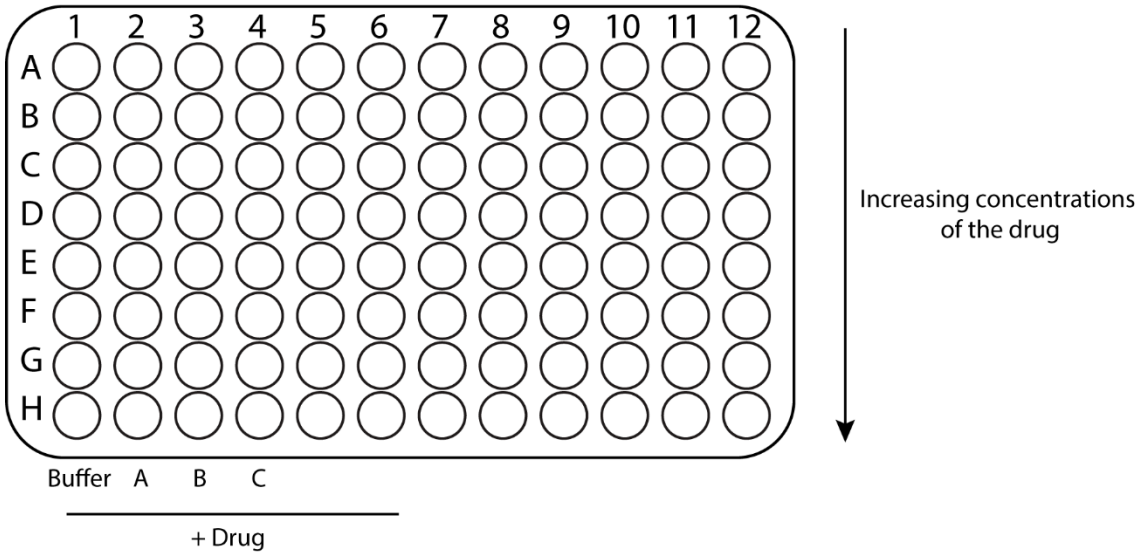

9.

Figure 9. ***96-well plate template for chemosensitization assays.*** *Increasing concentrations of each drug are added through the columns. Buffer and different molecules (represented in the picture as A, B, C…) were combined with the main (s) drug(s) used in the clinic.*

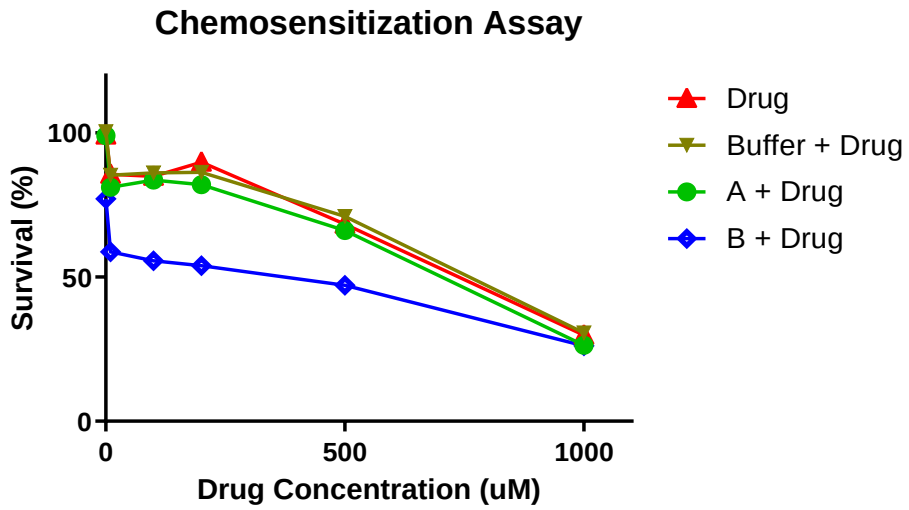

10.

Figure 10. ***Chemosensitization assay results.*** *Representative results after a chemosensitization assay. As showed in the figure, no effect was seen between drug alone and buffer or molecule A. However, molecule B has a strong effect sensitizing the cells to the treatment with the drug.*

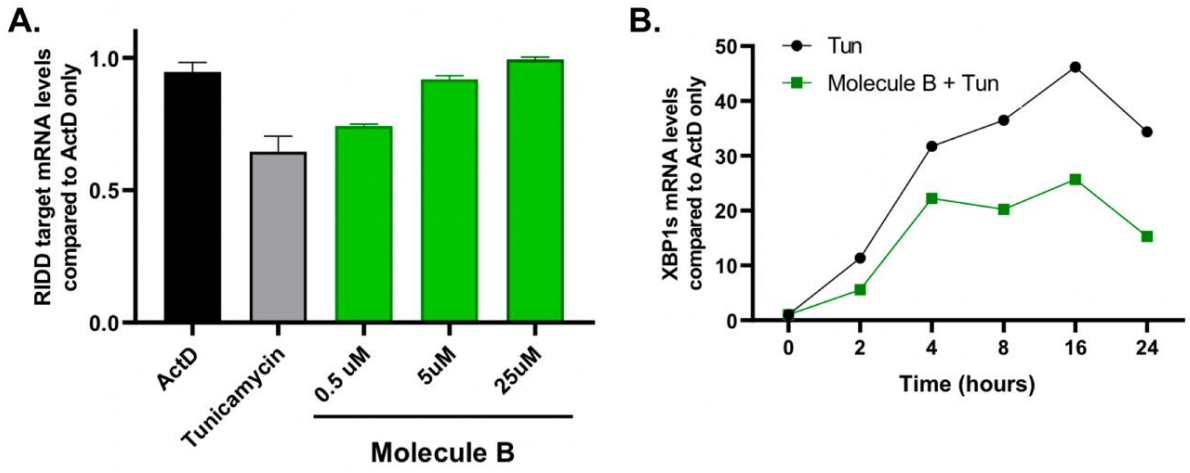

Figure 11. ***mRNA levels determination for XBP1s and RIDD targets.*** *Representative results of qPCR assay. Panel* ***A.*** *shows the increasing of degradation of RIDD mRNA levels after the treatment with tunicamycin (Tun). The inhibition of degradation is dose-dependent after the treatment with molecule.* ***B.*** *A time course treatment with Tunicamycin (black line) and Tunicamycin with molecule B (green line) was performed for 24 h. Molecule B inhibits the splicing of XBP1 mRNA induced by Tunicamycin*.